Current-driven spiral domain wall in a ferrimagnet near the magnetization compensation point

Jia-Lin Liu, Peng-Bin He [*], and Meng-Qiu Cai
School of Physics and Electronics, Hunan University, Changsha 410082, China

A spiral domain wall emerges when the Dzyaloshinskii-Moriya vector is along the easy axis. While the ferromagnetic spiral wall has been well studied, its ferrimagnetic counterpart has nevertheless not been explored. Here, using the collective variable approach, we derive the spiral domain-wall solutions in a ferrimagnetic nanostrip with a longitudinal easy axis and a bulk Dzyaloshinskii-Moriya interaction. At the magnetization compensation point, the wall rotates and propagates steadily in a wide current range. The (angular) velocity of this wall increases almost linearly with the experimentally feasible currents. Also, the wall exhibits a relativistic-like contraction with increasing velocity. Near this point, the wall moves smoothly with its velocity linearly depending on the current below the Walker breakdown. Above this critical current, all the internal parameters of the wall, such as the azimuthal angle, width, and spiral pitch, as well as their rates of change, oscillate periodically. The wall moves forward with its velocity varying periodically. These different behaviors at or near the compensation point are ascribed to the tunable demagnetization effect. The adjustability of FiM parameters, combining with the twist induced by the Dzyaloshinskii-Moriya interaction, can effectively change the DW's propagation and rotation.

I. INTRODUCTION

Current-driven magnetic domain walls (DWs) have spurred intensive research for fundamental interests in the nonlinear magnetism and potential applications in the logic operation [1] and data storage [2]. Along with an upsurge of investigation on the ferromagnetic DWs, growing attention has been drawn on the antiferromagnetic DWs driven by spin-transfer torques (STTs) [3–9] and spin-orbit torques [9–13], which have faster velocity and more stable structure. To overcome the difficulties in detecting and manipulating antiferromagnetic states, ferrimagnets (FiMs) provide a promising direction to combine the ultrafast dynamics and improved controllability. Moreover, in FiMs the magnetization and the spin density can be tuned by changing the chemical composition or the temperature [14]. These merits have led to a rise in experimental [15–20] and theoretical [21–28] studies of the FiM DWs, especially, those driven by the spin-orbit torques [16–19,24–27] and STTs [20,28].

Current research focuses on the FiM DWs in the vicinity of angular momentum compensation point, which can provide fast and efficient control of the DWs [29]. But so far no analytic study has been demonstrated of the FiM DWs near the magnetization compensation point (MCP) and with the Dzyaloshinskii-Moriya interaction (DMI). Despite the rela-

tive weakness, DMI influences the structure and movement of DWs remarkably. If the DM vector coincides with the easy axis, a spiral DW is allowed [30,31]. Otherwise, DMI results in a stabilization of homochiral DWs [32,33] and an enhancement of the Walker limit [34]. Recently, a significant DMI was observed in single thin FiM films [35]. Moreover, an adjustable bulk DMI was identified in amorphous FiM alloys [36]. These findings open an avenue toward the DM DWs in FiMs. In view of the well adjustability of FiM parameters, the FiM DWs may be of practical interest. However, the spiral DWs in FiM are still unexplored, which we will analyze theoretically.

Here we analyze the dynamics of DWs by employing the collective coordinates method, originally proposed by Slonczewski in 1970s [37]. Although this method seldom provides a quantitative fit to the real situations, it helps to get the key physical features with qualitative clarity. The early treatment was to view the central position (q) and the azimuthal angle of magnetization (ϕ) of the DW as two collective coordinates, often called q-ϕ model. In the past 20 years, by introducing the DW width parameter (Δ) as a dynamic variable, a generalized q-ϕ-Δ model often has been used [12,38,39]. For the spiral DW, to describe the dynamics completely, another new time-varying coordinate (Γ) was involved, leading to the q-ϕ-Δ-Γ model [40]. Here $2\pi/\Gamma$ is the screw pitch. Although the rates of change of Δ and Γ are usually minimal, it is necessary to treat them as collective coordinates for getting a complete and dynamic expressions of them, instead of the static ones usually used in q-ϕ model.

This work is structured as follows. The model and equations are introduced in Sec. II. In Sec. III an exact analytical solution is presented and analyzed for the spiral DW at MCP.
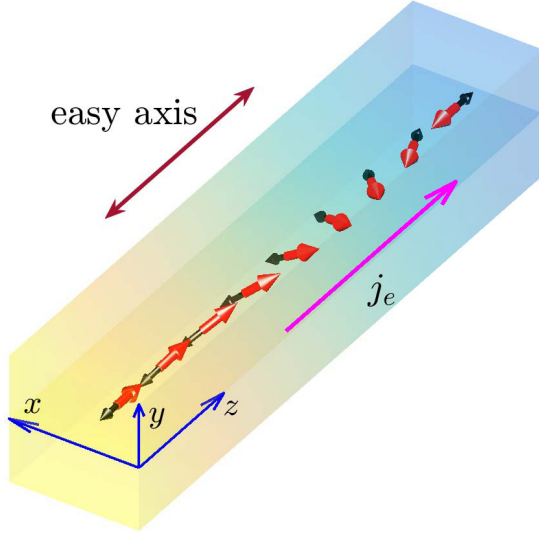
---

[*]hepengbin@hnu.edu.cn

FIG. 1. Schematic diagram of the DW profile. The black and red arrows represent the magnetic moments in two sublattices. The plane in the strip indicates the locations of magnetic moments.

In Sec. IV, near MCP, the dynamics of DW is solved by variational method. Finally, we end with conclusions in Sec. V.

II. MODEL AND EQUATIONS

As shown in Fig. 1, we consider a FiM metallic nanostrip with a bulk DMI and a longitudinal easy axis defined as z axis. The system is composed of two inequivalent sublattices, with magnetic moment densities $\mathbf{M}_{1,2}$. A longitudinal electric current flows through the strip, generating adiabatic and nonadiabatic STTs [41–43] exerted on the magnetic moments. In general, it is convenient to deploy transformation of variables from $\mathbf{M}_{1,2}$ to $\mathbf{l}$ and $\mathbf{m}$, where $\mathbf{m} = 1/2(\mathbf{M}_1/M_1 + \mathbf{M}_2/M_2)$ is the reduced magnetization, and $\mathbf{l} = 1/2(\mathbf{M}_1/M_1 - \mathbf{M}_2/M_2)$ is the staggered order parameter, with $M_{1,2}$ being the magnitudes of magnetization in two sublattices. $\mathbf{l}$ and $\mathbf{m}$ are subjected to the constraints $\mathbf{l} \cdot \mathbf{m} \equiv 0$ and $\mathbf{l}^2 + \mathbf{m}^2 \equiv 1$. In the ground state, $\mathbf{M}_1$ and $\mathbf{M}_2$ remain antiparallel. So $\mathbf{m} = 0$ and $|\mathbf{l}| = 1$. For the smooth nonuniform states, it is reasonable to assume $|\mathbf{m}| \ll 1$ and $|\mathbf{l}| \approx 1$ in the strong-exchange limit. To the first order in $\mathbf{m}$, considering the large antiferromagnetic coupling, the motion of $\mathbf{l}$ can be decoupled from $\mathbf{m}$. Then, by a tedious but direct derivation (see Appendix A for details), the two coupled Landau-Lifshitz-Gilbert equations about $\mathbf{M}_{1,2}$ are reduced to an equation about $\mathbf{l}$ [20,28,44,45],

$$\rho \mathbf{l} \times \frac{\partial^2 \mathbf{l}}{\partial t^2} - S_- \frac{\partial \mathbf{l}}{\partial t} + \alpha S_+ \mathbf{l} \times \frac{\partial \mathbf{l}}{\partial t} = -\mathbf{l} \times \frac{\delta E_l}{\delta \mathbf{l}} + \mathbf{T}_l, \quad (1)$$

where the parameters are defined by those of sublattices, $\rho = S_+^2/(8A_0)$, $S_\pm = S_1 \pm S_2$, and $\alpha = (\alpha_1 S_1 + \alpha_2 S_2)/(S_1 + S_2)$, with $\alpha_{1,2}$ being the sublattice damping constants. $S_{1,2} = M_{1,2}/\gamma_{1,2}$ is the densities of angular momentum in two sublattices with $\gamma_{1,2}$ being sublattice gyromagnetic ratios. $A_0 = \mathsf{J}/\Omega$ is the exchange energy density between nearest moments per unit cell, with $\mathsf{J} > 0$ being the exchange energy between a pair of nearest magnetic moments, and Ω the volume of unit cell.

The reduced magnetic energy functional $E_l = \int \mathcal{E}_l \, d\mathbf{r}$, with the energy density

$$\mathcal{E}_l = \frac{A_2}{2}\left(\frac{\partial \mathbf{l}}{\partial z}\right)^2 - K(\mathbf{l} \cdot \mathbf{e}_z)^2 - D\mathbf{e}_z \cdot \left(\mathbf{l} \times \frac{\partial \mathbf{l}}{\partial z}\right)$$
$$+ \frac{1}{2}\mu_0 M_-^2 [N_x(\mathbf{l} \cdot \mathbf{e}_x)^2 + N_y(\mathbf{l} \cdot \mathbf{e}_y)^2], \quad (2)$$

where the first term is the exchange energy density, and the exchange stiffness $A_2 = A_0 a^2/2$ with a being the lattice constant. The second term is the anisotropy energy density, and $K = K_1 + K_2$ where $K_{1,2} = \mathsf{K}_{1,2}/\Omega$ are the sublattice anisotropy constants, with $\mathsf{K}_{1,2}$ being the anisotropy energy per moment. The third term is the bulk DMI energy density, and $D = (\mathsf{D}/\Omega)a$ representing the strength of DMI [35,36], with D being the DMI energy per bond. The forth term is the demagnetization energy density with μ_0 being the vacuum permeability, and $N_{x,y}$ being the demagnetization factors along the x and y axes. For a long magnetic nanostrip, $N_z = 0$ and $N_x + N_y = 1$. Finally, $M_- = M_1 - M_2$.

After transformation (see Appendix A for details), the adiabatic and nonadiabatic STTs in Eq. (1) are expressed as

$$\mathbf{T}_l = -P_- j_e \frac{\partial \mathbf{l}}{\partial z} + \beta P_+ j_e \mathbf{l} \times \frac{\partial \mathbf{l}}{\partial z}, \quad (3)$$

where j_e is the current density and β is the nonadiabatic STT parameter. $P_\pm = P_1 \pm P_2$, where $P_{1,2} = \frac{\hbar}{2e}p_{1,2}$ with $\hbar$ being the reduced Planck constant, e the elementary charge, and p_i the spin polarizations of two sublattices.

Strictly speaking, the exchange and DMI energies depend on the gradient of magnetization. Here we consider a film with its width and thickness being smaller than the exchange length. Furthermore, the length scale of DMI (e.g., the spiral pitch defined in next section) is general much larger than the exchange length. Thus, the magnetization is assumed to be constant in the transverse direction.

In addition, the reduced magnetization $\mathbf{m}$ acts as a slave vector, which can be obtained by (see Appendix A for details)

$$\mathbf{m} = -\frac{S_+}{8A_0}\mathbf{l} \times \frac{\partial \mathbf{l}}{\partial t} - \frac{A_1}{4A_0}\frac{\partial \mathbf{l}}{\partial z} \quad (4)$$

with $A_1 = A_0 a$.

To illustrate our analytic results, we do some theoretical estimations by choosing typical parameters [15,20,28] in the following sections. Several magnetic parameters are listed as: $\gamma_1 = 1.94 \times 10^{11}$ s^{-1} T^{-1} and $\gamma_2 = 1.76 \times 10^{11}$ s^{-1} T^{-1}, $\mathsf{K}_1 = \mathsf{K}_2 = 0.3$ meV, $\mathsf{J} = 7.5$ meV, $\mathsf{D} = 0.3$ meV, and $\alpha_1 = \alpha_2 = 0.004$. The sublattice magnetization can be adjusted by the temperature [20]. The lattice constant $a = 0.4$nm, and the volume of unit cell is approximated as $\Omega = a^3$. For the rare earth-transition metal FiMs, the spin polarization is mostly determined by the transition metal sublattice. So the spin polarizations $p_1 = 0.11$ and $p_2 = 0$ [20].

III. DYNAMICS AT MCP

At MCP, the two sublattices have equal magnetization. So $M_1 = M_2$, and the demagnetization energy vanishes. In this case a static spiral DW solution can be strictly derived by minimizing the magnetic energy [Eq. (2)]. Assuming a constant

magnitude, it is convenient to parametrize $\mathbf{l}$ by spherical coordinates, namely, $\mathbf{l} = \sin\theta\cos\varphi\mathbf{e}_x + \sin\theta\sin\varphi\mathbf{e}_y + \cos\theta\mathbf{e}_z$ with θ and φ being the polar and azimuthal angles, respectively. Then a local minima of the energy functional (2) is a static spiral DW [30,31] expressed as $\theta = 2\arctan\exp[\lambda(z - q)/\Delta_s]$, and $\varphi = \Gamma_s(z - q) + \phi$, where $\lambda = \pm 1$ allows distinguishing between a head-to-head DW ($\lambda = 1$) or a tail-to-tail DW ($\lambda = -1$). q is the center position of DW, and ϕ is the tilted angle of the center magnetic moment. The DW width $\Delta_s = (\Delta_i^{-2} - \Gamma_s^2)^{-1/2}$ with $\Delta_i = \sqrt{A_2/(2K)}$ being the width

in the absence of DMI. $\Gamma_s = D/A_2$ with $2\pi/\Gamma_s$ being the pitch of spiral. Obviously, this DW exists for weak DMI ($D < \sqrt{2KA_2}$), namely, $\Gamma_s\Delta_i < 1$.

At MCP, we have obtained an exact solution having the form of static spiral Walker profile. Based on this static DW profile, it is assumed that a traveling-wave ansatz takes the form of $\theta = \theta(\xi)$, and $\varphi = \Gamma\xi + \phi(t)$ with $\xi = z - q(t)$. $q(t)$ and $\phi(t)$ are two dynamic variables, representing the center position and the tilted angle of DW. Inserting this ansatz into the θ-φ form of Eq. (1) without the demagnetization term, we have

$$[\rho(\Gamma\dot{v} - \dot{\omega}) + \alpha S_+(\Gamma v - \omega) + \beta P_+ j_e \Gamma]\sin\theta + (S_- v + P_- j_e)\theta_\xi = -2[(A_2 - \rho v^2)\Gamma - (D - \rho v\omega)]\cos\theta\,\theta_\xi, \quad (5)$$

$$[S_-(\Gamma v - \omega) + P_- j_e \Gamma]\sin\theta - (\rho\dot{v} + \alpha S_+ v + \beta P_+ j_e)\theta_\xi = (A_2 - \rho v^2)\theta_{\xi\xi} - [2K + A_2\Gamma^2 - 2D\Gamma + \rho(\Gamma\dot{v} - \dot{\omega})]\sin\theta\cos\theta, \quad (6)$$

where the subscript ξ indicates the derivative with respect to it, and the overdot denotes the derivative with respect to the time. It is easy to observe that, if taking $\theta_\xi \propto \sin\theta$, Eqs. (5) and (6) may be solved consistently.

Equating the coefficients of $\sin\theta\cos\theta$ in Eq. (6), we obtain

$$\theta_\xi = \frac{\lambda}{\Delta}\sin\theta, \quad (7)$$

where $\Delta = \Delta_s(1 - v^2/v_{sw}^2)^{1/2}[1 + (\Gamma - \Gamma_s)^2\Delta_s^2 + (\Gamma\dot{v} - \dot{\omega})\Delta_s^2/v_{sw}^2]^{-1/2}$, with $v = \dot{q}$ being the velocity, $\omega = \dot{\phi}$ the angular velocity, and $v_{sw} = \sqrt{A_2/\rho}$ the spin-wave velocity. Solving Eq. (7) yields the dynamic Walker solution.

Furthermore, equating the coefficients of $\sin\theta\cos\theta$ in Eq. (5), Γ is derived as $\Gamma = (\Gamma_s - v\omega/v_{sw}^2)/(1 - v^2/v_{sw}^2)$. Then the dynamic spiral DW is described by

$$\theta = 2\arctan\exp\left[\lambda\frac{z - q(t)}{\Delta}\right], \quad (8)$$

$$\varphi = \Gamma[z - q(t)] + \phi(t). \quad (9)$$

Finally, equating the coefficients of $\sin\theta$ in Eqs. (5) and (6), the dynamic equations of v and ω are obtained,

$$\rho\begin{pmatrix}\dot{v}\\\dot{\omega}\end{pmatrix} = \begin{pmatrix}a_{11} & a_{12}\\a_{21} & a_{22}\end{pmatrix}\begin{pmatrix}v\\\omega\end{pmatrix} + \begin{pmatrix}b_1\\b_2\end{pmatrix}j_e, \quad (10)$$

where $a_{11} = \lambda\Gamma\Delta S_- - \alpha S_+$, $a_{12} = -\lambda\Delta S_-$, $a_{21} = \lambda(1 + \Gamma^2\Delta^2)S_-/\Delta$, $a_{22} = -(\lambda\Gamma\Delta S_- + \alpha S_+)$, $b_1 = \lambda\Gamma\Delta P_- - \beta P_+$, and $b_2 = \lambda(1 + \Gamma^2\Delta^2)P_-/\Delta$. For the steady motion, both the acceleration $\dot{v}$ and the angular acceleration $\dot{\omega}$ vanish. Therefore, the velocity and angular velocity are expressed as

$$v_0 = \frac{\Gamma_0\Delta_0}{1 + \Gamma_0^2\Delta_0^2}\Delta_0\omega_0 - Ej_e, \quad (11)$$

$$\omega_0 = \lambda(1 + \Gamma_0^2\Delta_0^2)F\frac{j_e}{\Delta_0}, \quad (12)$$

where

$$E = \frac{S_-P_- + \alpha\beta S_+P_+}{S_-^2 + \alpha^2 S_+^2}, \quad (13)$$

$$F = \frac{\alpha S_+P_- - \beta S_-P_+}{S_-^2 + \alpha^2 S_+^2}. \quad (14)$$

Δ_0 and Γ_0 are written as

$$\Delta_0 = \Delta_s\sqrt{\frac{1 - v_0^2/v_{sw}^2}{1 + (\Gamma_0 - \Gamma_s)^2\Delta_s^2}}, \quad (15)$$

$$\Gamma_0 = \frac{\Gamma_s - v_0\omega_0/v_{sw}^2}{1 - v_0^2/v_{sw}^2}. \quad (16)$$

In general, under small perturbations, a physical solution must be stable. This can be explored by the linearization method. Inserting $v = v_0 + v'$ and $\omega = \omega_0 + \omega'$ into Eq. (10), and retaining only the first-order terms with respect to the perturbations v' and ω', we can obtain the linearized equations. Then, solving for solutions of the form $v'(\omega') \propto e^{\kappa t}$, we can get a secular equation

$$\rho^2\kappa^2 + 2\alpha S_+\rho\kappa + S_-^2 + \alpha S_+^2 = 0, \quad (17)$$

which has the roots

$$\kappa_\pm = -\alpha\frac{S_+}{\rho} \pm i\frac{S_-}{\rho}. \quad (18)$$

Obviously, the real parts of $\kappa_\pm$ are negative. So this steady DW is stable.

Although there are no explicit relations between the dynamic variables and the currents, several significative conclusions can be drawn from above calculations. More abundant dynamics comes forth due to the good adjustability of FiM. For example, $S_\pm$ and $P_\pm$ in Eqs. (13) and (14) can be tuned by temperature or by choosing different materials.

First, the magnetic moments can rotate clockwise or anticlockwise ($\omega_0 > 0$ or < 0), depending on the DW type ($\lambda = \pm 1$) and the sign of $\alpha S_+P_- - \beta S_-P_+$. From Eq. (12), the angular velocity increases in the presence of DMI with the increment proportional to the square of the twist $\Gamma_0\Delta_0$.

Second, the propagation of DW is also greatly affected by combining the twist produced by DMI and the tunability of FiM. From Eq. (11), in the absence of DMI ($\Gamma_0 = 0$), $v_0 = -(S_-P_- + \alpha\beta S_+P_+)/(S_-^2 + \alpha^2 S_+^2)j_e$, independent of the topological charge λ. Considering that $\alpha\beta \ll 1$ generally, whether the DW moves against or along the current direction mostly depends on the sign of S_-P_-, which is determined by the parameters of two sublattices. This is different
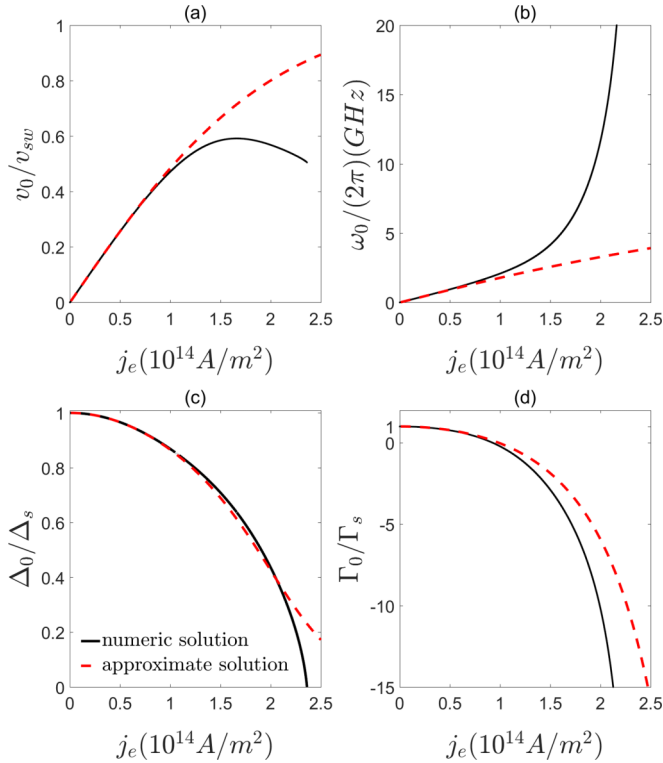
FIG. 2. Dependence of v_0 (a), ω_0 (b), Δ_0 (c), and Γ_0 (d) on the current density for the steady DW at MCP. The solid curves are plotted by numerically solving Eqs. (11), (12), (15), and (16). The dashed curves are from Eqs. (19) and (20). $M_1 = M_2 = 5.25 \times 10^5$ A/m [20]. The nonadiabatic parameter $\beta = 0.53$ [20]. The DW type is chosen as $\lambda = 1$.

from ferromagnets, where the DW always moves against the current [30] without DMI. On the other hand, depending on whether the DW rotates in the same or opposite direction as the twist of DW, DMI can speed up or slow down the DW. This behavior is similar to the ferromagnetic case [30], but not exactly the same. DMI-induced increment and reversal of v_0 relies on $\alpha - \beta$ for ferromagnetic DWs, while it depends on $\alpha S_+ P_- - \beta S_- P_+$ for FiM DWs. In comparison, the latter is more tunable. Especially, if $\alpha S_+ P_- \approx \beta S_- P_+$, the DW almost stops rotating and propagates fluently.

Third, the chirality of spiral can be switched possibly. The chirality refers to the sense of spatial rotation, corresponding to the positive or negative Γ_0. For a static spiral DW, the sign of Γ_s is determined by the direction of DM vector. For a steady spiral DW, its propagation and rotation happen simultaneously, describing by the velocity v_0 and the angular velocity ω_0. Like the DW width (Δ_0), the spiral pitch (Γ_0) also varies when a DW moves steadily. From Eq. (16), Γ_0 not only varies along with the propagation and rotation of DW, but also changes sign at $v_0 \omega_0 / v_{sw}^2 = \Gamma_s$. When the chirality is reversed, the DW twist ($\Gamma_0 \Delta_0$) also changes sign. From Eq. (11), the variation trend of velocity is altered. Also by comparing the solid curves in Fig. 2(a) and Fig. 2(d), at the current density $j_e \approx 9.12 \times 10^{13}$ A/m^2, Γ_0 changes sign, and the increase of velocity starts to slow down, then decreases with the current increasing further.

Finally, from Eqs. (11), (12), (15), and (16), we can infer the counterpart relations of v_0, ω_0, Δ_0 and Γ_0 with j_e for ferromagnets and antiferromagnets. If setting $S_2 = P_2 = 0$, the system becomes ferromagnetic: $S_+ = S_-$ and $P_+ = P_-$. Then $v_0 \propto [\lambda \Gamma_0 \Delta_0 (\alpha - \beta) - (1 + \alpha\beta)]/(1 + \alpha^2)j_e$, and $\omega_0 \propto \lambda(\alpha - \beta)/(1 + \alpha^2)j_e$, which are just the results of the ferromagnetic spiral DW in Ref. [30]. Additionally, if setting $S_1 = S_2 = S$, and $P_1 = P_2 = P$, the system is antiferromagnetic. Then $S_+ = 2S$, $S_- = 0$, $P_+ = 2P$, and $P_- = 0$. The steady-state velocity $v_0 = -(\beta/\alpha)(P j_e / S)$. The angular velocity vanishes.

It must be pointed out that Eqs. (11), (12), (15), and (16) are coupled transcendental equations. It is difficult to see a direct dependence of these DW parameters on the current. However, due to the strong exchange interaction, the spin-wave velocity is very high (about 2.64×10^4 m/s for the adopted magnetic parameters). So it is not a bad approximation to take a limit that $v_0 \ll v_{sw}$. By keeping the leading-order terms of v_0/v_{sw}, Eqs. (11), (12), (15), and (16) can be decoupled. Then, we obtain the explicit dependence of v_0 and ω_0 on the current density,

$$v_0 = -\frac{v_{sw}^2 + Aj_e^2 - \sqrt{(v_{sw}^2 + Aj_e^2)^2 - Bv_{sw}^2 j_e^2}}{C j_e}, \quad (19)$$

$$\omega_0 = -\Gamma_s \frac{2v_{sw}^2 - Aj_e^2 - 2\sqrt{(v_{sw}^2 + Aj_e^2)^2 - Bv_{sw}^2 j_e^2}}{C j_e}, (20)$$

where

$$A = \lambda F \big[2E\Gamma_s \Delta_s + \lambda F \big(1 - \Gamma_s^2 \Delta_s^2\big) \big], \quad (21)$$

$$B = 6\lambda F \Gamma_s \Delta_s (E - \lambda F \Gamma_s \Delta_s), \quad (22)$$

$$C = 3\lambda F \Gamma_s \Delta_s, \quad (23)$$

with E and F being Eqs (13) and (14). Inserting Eqs. (19) and (20) into Eqs. (15) and (16), we can also derive the explicit dependence of Δ_0 and Γ_0 on j_e.

To corroborate the reliability of above approximate analytical results, we plot v_0, ω_0, Δ_0, and Γ_0 in Fig. 2 as a function of j_e by solving Eqs. (11), (12), (15), and (16) numerically. Comparing with the dashed curves directly plotted from Eqs. (19) and (20), the validity of the approximation is confirmed for an experimentally feasible current range ($j_e \lesssim 10^{14}$A/m^2 in Fig. 2).

In general, the spin-wave velocity v_{sw}, which is very high, defines an upper limit for the DW motion. There are two obstacles to arrive at v_{sw}. One is the Joule heat generated by a high current. The other is the destruction of DW before its velocity arrives at v_{sw}. This is ascribed to the fact that ω_0 and Γ_0 approach infinity when $j_e \gtrsim 2.35 \times 10^{14}$ A/m^2 [see Figs. 2(b) and 2(d)]. Moreover, Δ_0 has been close to zero before v reaches v_{sw}, as observed by comparing Figs. 2(a) and 2(c). So, in this high-current range, the solution is not physical. So far as we know, the typical current density in these kinds of experiments is lower than several TA/m^2 [16–20]. Therefore, though the velocity can approach the order of magnitude of v_{sw} theoretically, it is difficult to reach so high current experimentally. However, the spin transfer torque is pro-

portional to j_e/M_s [42]. If choosing a material with small saturation magnetization, the current can be decreased possibly.

IV. DYNAMICS NEAR MCP

Once the system deviates from MCP [20], the demagnetization term can not be omitted in Eq. (2). It is impossible to get a rigorous solution of DW. However, near MCP, the demagnetization term $1/2\mu_0 M_-^2$ is small. So it is reasonable to suppose the static spiral DW profile is preserved when including the STTs, the damping, and the demagnetization energy. Moreover, the DW dynamics is governed by four collective coordinates $q(t)$, $\phi(t)$, $\Delta(t)$, and $\Gamma(t)$, which evolution equations can be obtained by a perturbation method [30] or a variational method [37].

Here we use the variational method [37] to derive the dynamic equations about the collective coordinates. The dynamic ansatz has the same form as the static spiral Walker profile, just regarding q, ϕ, Δ, and Γ as dynamic variables. For convenience, Eq. (1) is written in a variational form, $\delta E_l = \frac{\delta E_l}{\delta \theta}\delta\theta + \frac{\delta E_l}{\delta \varphi}\delta\varphi$, where $\delta E_l/\delta\theta = -\rho(\theta_{tt} - \varphi_{tt}\sin\theta\cos\theta) - \alpha S_+\theta_t + S_-\varphi_t\sin\theta - (P_-\varphi_z\sin\theta - \beta P_+\theta_z)j_e$, and $\delta E_l/\delta\varphi = -\rho(\varphi_{tt}\sin^2\theta + 2\theta_t\varphi_t\sin\theta\cos\theta) - S_-\theta_t\sin\theta - \alpha S_+\varphi_t\sin^2\theta + (P_-\theta_z\sin\theta + \beta P_+\varphi_z\sin^2\theta)j_e$. Integrating δE_l over z and using the dynamic Walker ansatz, the variation of DW energy per unit area, $\delta\sigma = \int \delta E_l\, dz$, can be obtained after a straightforward but rather tedious algebra manipulation (see Appendix B for detailed derivations). Then the dynamic equations about q, ϕ, Δ and Γ read

$$\frac{\delta\sigma}{\delta q} = -2\rho(1+\Gamma^2\Delta^2)\Delta^{-1}\ddot{q} + 2\rho\Gamma\Delta\ddot{\phi} + \rho\Delta\ddot{\Gamma} - 2\alpha S_+(1+\Gamma^2\Delta^2)\Delta^{-1}\dot{q} - 2(\lambda S_- - \alpha S_+\Gamma\Delta)\dot{\phi}$$
$$- 2\rho\Gamma\Delta\dot{q}\dot{\Gamma} - 2\rho(\Gamma^2-\Delta^{-2})\dot{q}\dot{\Delta} + 2\rho\Gamma\dot{\phi}\dot{\Delta} - 2(1+\Gamma^2\Delta^2)\Delta^{-1}\beta P_+ j_e, \tag{24}$$

$$\frac{\delta\sigma}{\delta\phi} = 2\rho\Gamma\Delta\ddot{q} - 2\rho\Delta\ddot{\phi} + 2(\lambda S_- + \alpha\Gamma\Delta S_+)\dot{q} - 2\alpha S_+\Delta\dot{\phi} + 2\rho\Delta\dot{q}\dot{\Gamma} + 2\rho\Gamma\dot{q}\dot{\Delta} - 2\rho\dot{\Delta}\dot{\phi} + 2(\lambda P_- + \Gamma\Delta\beta P_+)j_e, \tag{25}$$

$$\frac{\delta\sigma}{\delta\Delta} = -\rho\Gamma\ddot{q} - \rho\ddot{\phi} - \frac{\pi^2}{6}\rho\Delta^{-1}\ddot{\Delta} - \rho\Delta^{-2}\dot{q}^2 + \frac{\pi^2}{12}\rho\Delta^{-2}\dot{\Delta}^2 - \frac{\pi^2}{6}\alpha S_+\Delta^{-1}\dot{\Delta} - \frac{\pi^2}{6}\lambda S_-\Delta\dot{\Gamma} - 2\rho\dot{q}\dot{\Gamma}, \tag{26}$$

$$\frac{\delta\sigma}{\delta\Gamma} = -\frac{\pi^2}{6}\rho\Delta^3\ddot{\Gamma} + 2\rho\Gamma\Delta\dot{q}^2 + \frac{\pi^2}{6}\lambda S_-\Delta\dot{\Delta} - \frac{\pi^2}{6}\alpha S_+\Delta^3\dot{\Gamma} - \frac{\pi^2}{2}\rho\Delta^2\dot{\Gamma}\dot{\Delta} - 2\rho\Delta\dot{q}\dot{\phi}. \tag{27}$$

In addition, inserting the dynamic Walker ansatz into the magnetic energy density [Eq. (2)] and integrating over z, we can get the DW energy per unit area,

$$\sigma = \Delta\left\{A_2(\Delta^{-2}+\Gamma^2) + 2K - 2D\Gamma + \frac{1}{2}\mu_0 M_-^2 \times \left[1 + (N_x - N_y)\frac{\pi\Gamma\Delta}{\sinh(\pi\Gamma\Delta)}\cos 2\phi\right]\right\}. \tag{28}$$

Equations (24), (26), and (27) represent dynamic pressures due to the changes of the location, width, and pitch of DW. Equation (25) represents a dynamic torque due to the rotation of magnetic moments. These dynamic pressures and torque can be balanced by corresponding static ones, which are derived from the variational derivatives of σ [Eq. (28)] with respect to q, ϕ, Δ, and Γ.

The DW energy σ is translation invariant, namely, σ is independent of q. So the dynamics of steady DW can be obtained by setting $\ddot{q}$, $\ddot{\phi}$, $\ddot{\Delta}$, $\ddot{\Gamma}$, $\dot{\phi}$, $\dot{\Delta}$, and $\dot{\Gamma}$ to zero. Then, from Eqs. (24), (25), and (28), we get the steady-state velocity,

$$v_0 = \dot{q} = -\frac{\beta}{\alpha}\frac{P_+}{S_+}j_e, \tag{29}$$

and the DW angle ϕ_0 which satisfies

$$\sin 2\phi_0 = \lambda\frac{j_e}{j_0}, \tag{30}$$

where

$$j_0 = \frac{1}{2}(N_x - N_y)\frac{\alpha S_+\mu_0 M_-^2}{\beta S_- P_+ - \alpha S_+ P_-}\frac{\pi\Gamma_0\Delta_0^2}{\sinh(\pi\Gamma_0\Delta_0)}. \tag{31}$$

From Eqs. (26), (27), and (28), the steady solutions Δ_0 and Γ_0 can be obtained. By omitting the terms of $\mu_0 M_-^2$, near MCP,

which is much smaller than other terms, Δ_0 and Γ_0 read (see Appendix B for detailed derivations)

$$\Delta_0 = \Delta_s \frac{\left(1 - v_0^2/v_{sw}^2\right)^{3/2}}{\sqrt{\left(1 - v_0^2/v_{sw}^2\right)^2 + \Gamma_s^2\Delta_s^2 v_0^4/v_{sw}^4}}, \tag{32}$$

$$\Gamma_0 = \frac{\Gamma_s}{1 - v_0^2/v_{sw}^2}. \tag{33}$$

Inserting Eq. (29) into Eqs. (32) and (33), Δ_0 and Γ_0 are expressed as explicit functions of j_e. Further substituting Δ_0 and Γ_0 into Eq. (31), ϕ_0 can also be written as a function of j_e. In the absence of DMI, $\Gamma_s = 0$. $\Delta_0 = \Delta_s\sqrt{1 - v_0^2/v_{sw}^2}$. When the DW moves faster, it contracts in a relativistic-like manner, similar to its antiferromagnetic counterpart.

When $|j_e/j_0| > 1$, Eq. (30) has no physical solution and the steady DW becomes unstable (known as the Walker breakdown). Inserting $j_e = \pm j_0$ and $v = \mp\frac{\beta}{\alpha}\frac{P_+}{S_+}j_0$ into Eqs. (32) and (33), and eliminating Γ_0 and Δ_0 in Eq. (31), the magnitude of critical current j_c satisfies

$$j_c = j_\Delta\left(1 - v_c^2/v_{sw}^2\right)\frac{\pi f^2\Gamma_s\Delta_s^2/\Delta_i}{\sinh\left(\pi f\Gamma_s\Delta_s\right)}, \tag{34}$$

where

$$j_\Delta = \frac{1}{2}|N_x - N_y|\mu_0 M_-^2 \frac{\alpha S_+}{|\beta S_- P_+ - \alpha S_+ P_-|}\Delta_i \quad (35)$$

and

$$f = \frac{\sqrt{1 - v_c^2/v_{sw}^2}}{\sqrt{(1 - v_c^2/v_{sw}^2)^2 + \Gamma_s^2 \Delta_s^2 v_c^4/v_{sw}^4}}, \quad (36)$$

with $v_c = \frac{\beta}{\alpha} \frac{P_+}{S_+} j_c$. From Eq. (35), it is easy to observe that if $\beta S_- P_+ \approx \alpha S_+ P_-$, the critical current diverges and the velocity can be very large. This means that $1/\alpha(\gamma_2 M_1 - \gamma_1 M_2)/(\gamma_2 M_1 + \gamma_1 M_2) \approx 1/\beta(P_1 - P_2)/(P_1 + P_2)$. For ferromagnets, we can take $M_2 = 0$ and $P_2 = 0$. This equation is reduced as $\alpha \approx \beta$, which has been reported for ferromagnetic DWs [43]. It is difficult to control or adjust α and β in a well-defined manner and approach this limit. However, for FiMs, $M_{1,2}$ can be tuned by the temperature [20]. The parameters of STTs on the right of this equation can be varied by choosing different materials. So it is possible to postpone the Walker breakdown and acquire a high steady velocity.

Equation (34) is a transcendental equation about j_c, which can be solved in view of the strong exchange, namely, in the limit of $v_c \ll v_{sw}$. If omitting v_c^2/v_{sw}^2, $j_c/j_\Delta \propto \frac{\pi \Gamma_s \Delta_s}{\sinh(\pi \Gamma_s \Delta_s)}$, which is similar to the ferromagnetic result in Ref. [30]. Furthermore, it is more legitimate to keep the leading-order terms in v_c/v_{sw}, and the critical current density is explicitly expressed as

$$j_c = j_\Delta \frac{\sqrt{\frac{\Delta_i^2}{\Delta_s^2} + 2\eta^3 \cosh(\pi \Gamma_s \Delta_s)\frac{v_\Delta^2}{v_{sw}^2}} - \frac{\Delta_i}{\Delta_s}}{\eta^2 \cosh(\pi \Gamma_s \Delta_s)\frac{v_\Delta^2}{v_{sw}^2}}, \quad (37)$$

where $\eta = \frac{\pi \Gamma_s \Delta_s}{\sinh(\pi \Gamma_s \Delta_s)}$, and $v_\Delta = \frac{\beta}{\alpha} \frac{P_+}{S_+} j_\Delta$.

Let us briefly discuss the influence of DMI on the critical behavior. The static DW twist $\Gamma_s \Delta_s = D/\sqrt{2KA_2 - D^2}$, which demands that $D < \sqrt{2KA_2}$. The inset of Fig. 3 indicates that the twist is increased by DMI, and greatly enlarged when D approaches $\sqrt{2KA_2}$. This results in that the critical current is suppressed by DMI, as revealed by Fig. 3, which shows the dependence of j_c on D for several small v_Δ. As D is close to $\sqrt{2KA_2}$, the critical current vanishes gradually. On the other hand, if $D = 0$, $\Gamma_s = 0$ and $\Delta_s = \Delta_i$. Then $j_c \approx j_\Delta\sqrt{1 - v_\Delta^2/v_{sw}^2}$, as shown in the top right corner of Fig. 3. This limit value of j_c can be obtained from Eq. (34) or Eq. (37).

Beyond Walker breakdown ($|j_e| > j_c$), the DW enters the precessional regime. Unlike the ferromagnetic case [30], there is no analytic solution. Solving the dynamic equations [Eqs. (24)–(28)] numerically, we find that the collect coordinates ϕ, Δ and Γ, and their rates of change, as well as the velocity v, all depend on time periodically. To gain a further insight into above results, we plot the evolutions of the collective coordinates ϕ, Δ and Γ in Figs. 4(a), 4(b), and 4(c), respectively. The evolutions of the velocity, angular velocity, and rates of change of Δ and Γ are shown in Figs. 4(d), 4(e), 4(f), and 4(g). For comparison, we also plot the evolutions for $|j_e| < j_c$.

In the steady region ($|j_e| < j_c$), v, ϕ, Γ, and Δ reach steady values after a transient process. ω, $\dot{\Gamma}$, and $\dot{\Delta}$ approach zero
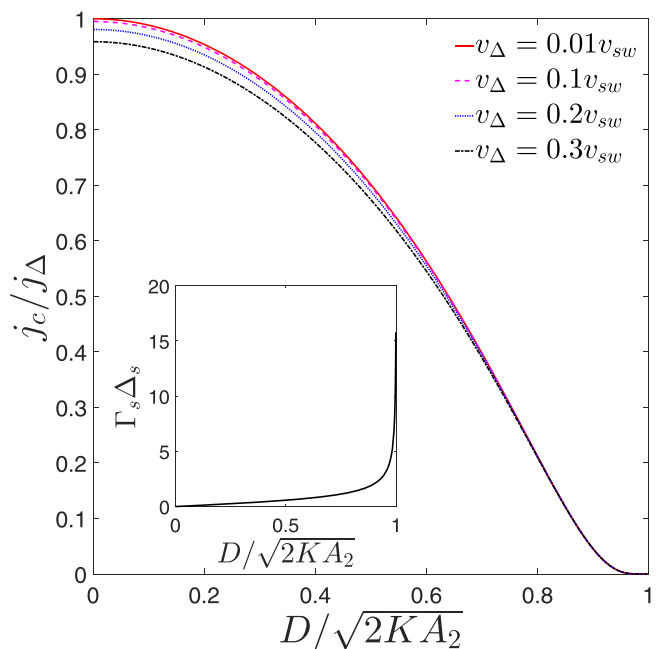

FIG. 3. Dependence of the critical current and the DW twist (inset) on the reduced DMI strength.

quickly. These evolution results coincide with the relation between v (ω) and j_e, as indicated by the dashed lines in Fig. 5. When $\beta = 0$, the steady DW stops moving.

In the precessional region ($|j_e| > j_c$), the DW angle ϕ, DW width Δ, and reciprocal of spiral pitch Γ vary periodically, with ϕ being twice the period of Δ and Γ, as shown in Figs. 4(a), 4(b), and 4(c). In addition, the deviations of Δ and Γ from their static values Δ_s and Γ_s are vanishingly small. This justifies a usual treatment neglecting the variation of Δ and Γ.

In addition, the rates of change of ϕ, Δ, and Γ vary periodically with the same period. Especially, $\dot{\Delta}$ and $\dot{\Gamma}$ oscillate around zero. So we can take time average of Eqs. (24)–(27) by neglecting the terms including $\dot{\Delta}$ and $\dot{\Gamma}$, due to the vanishing smallness of their time averages. Then we obtain the average velocity and angular velocity, which are formally identical to Eqs. (11) and (12) with Δ_0 and Γ_0 replaced by the corresponding static values. As shown by the dotted lines in Fig. 5, these analytic results exhibit a very good agreement with the numerical calculations (solid lines in Fig. 5) in the range of high currents. This agreement can be ascribed to the fact that the precession of the azimuthal angle [as shown in Fig. 4(a)] results in the vanishing of the demagnetization-induced terms after being averaged over time. Near the Walker breakdown, the analytic results deviate from the numeric ones a little more. So it is unsuitable to adopt the static values of Γ and Δ in deriving the average (angular) velocity in the critical region.

For the adopted parameters near MCP, $v_{sw} \approx 1.84 \times 10^4$ m/s. At the Walker breakdown, $v_c = -17.0$ m/s for $\beta = 0.53$, and 4.34 m/s for $\beta = -0.53$. So the velocity of steady DW is far less than v_{sw}. For the precessional DW, if the average velocity reaches v_{sw}, the current density should be 4.84×10^{13} A/m² for $\beta = 0.53$, 6.07×10^{13} A/m² for $\beta = 0$, and 8.14×10^{13} A/m² for $\beta = -0.53$. Under such a high
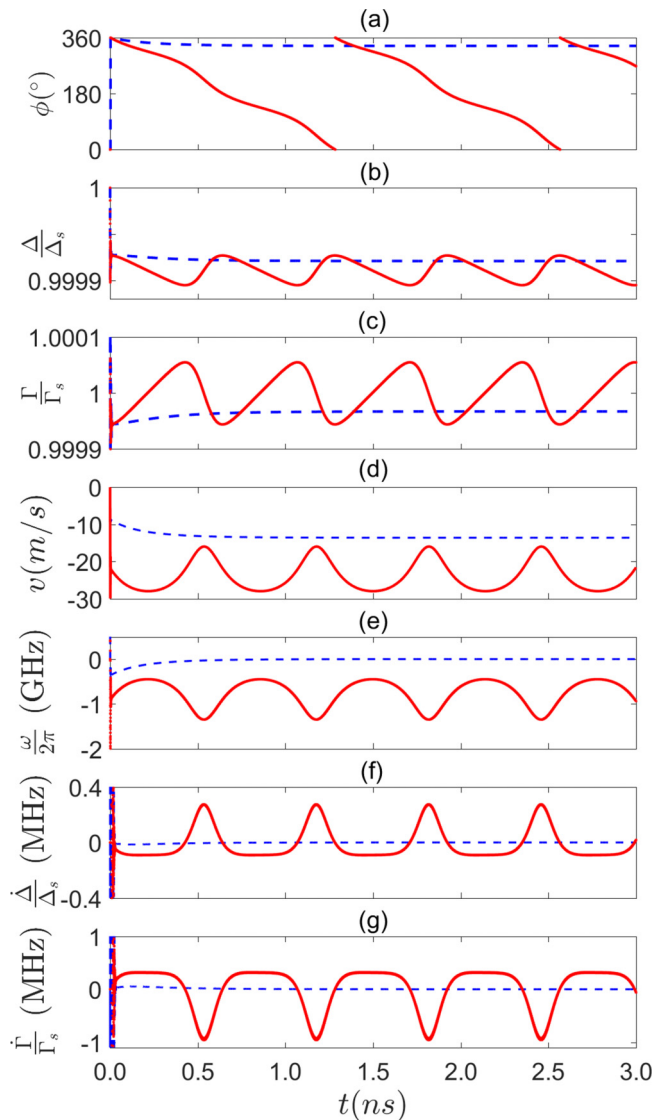
FIG. 4. Evolutions of the collective coordinates ϕ (a), Δ (b), and Γ (c), as well as the velocity v (d), the angular velocity ω (e), the rate of change of DW width $\dot{\Delta}$ (f), and the rate of change of spiral pitch $\dot{\Gamma}$ (g). The red solid curve corresponds to $j_e = 2j_c$, and the blue dashed curve $j_e = 0.8j_c$. $M_1 = 8 \times 10^5$ A/m and $M_2 = 7.09 \times 10^5$ A/m [20]. The nonadiabatic parameter $\beta = 0.53$ [20]. The DW type is chosen as $\lambda = 1$.

current, the oscillations of Δ and Γ become more dramatic but are still around their static values. So the analytic expression for average velocity is still valid. On the other hand, through changing the chemical composition or the temperature, the sublattice magnetization can be adjusted for enhancing the steady velocity.

It should be noted that the $\bar{\omega}$ vs j_e/j_c curve is independent of β, as shown in the inset of Fig. 5. This is because $\omega \propto \alpha S_+ P_- - \beta S_- P_+$ [see Eq.(12)] and $j_c \propto 1/(\alpha S_+ P_- - \beta S_- P_+)$ [see Eq. (35)]. The β dependence is offset. Above j_c, the DW not only moves sometimes fast and sometimes slow with the average velocity linearly increasing with the currents, but also rotates likewise.
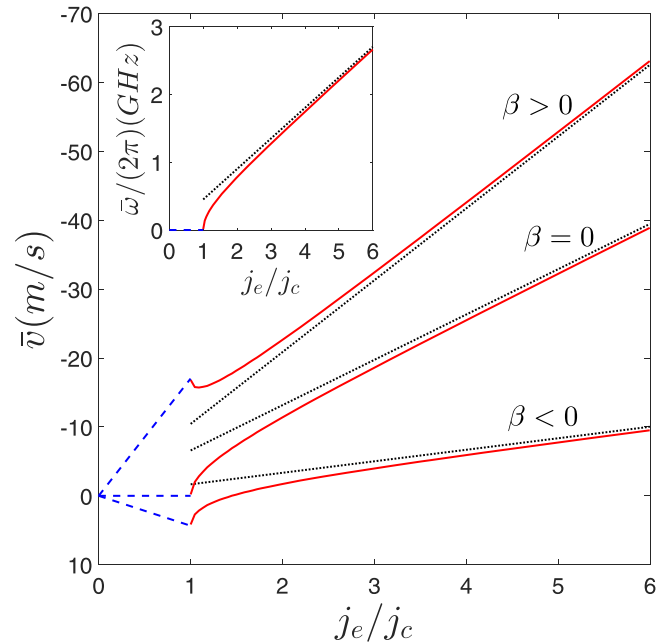

FIG. 5. Dependence of the velocity and the angular velocity (inset) on the current density. The blue dashed lines correspond to the steady DW. The red solid curves represent the average (angular) velocity of the precessional DW, which are plotted by solving Eqs. (24)–(27) numerically. The black dotted lines are from Eqs. (11) and (12) by taking $\Delta_0 = \Delta_s$ and $\Gamma_0 = \Gamma_s$. The parameters are the same as those in Fig. 4.

V. CONCLUSION

In this paper we have studied the DW dynamics driven by the adiabatic and nonadiabatic STTs in a ferrimagnetic nanostrip with a longitudinal easy axis and a bulk DMI. At the MCP, a spiral DW is obtained analytically using the traveling-wave ansatz. Owing to the vanishing of demagnetization effects, this DW moves steadily in a wide range of current. Its velocity and angular velocity are proportional to the current density in an experimentally feasible current range. Moreover, if the DW moves faster, it shrinks as $\sqrt{1 - v_0^2/v_{sw}^2}$.

Deviating from MCP, two motion regimes with different mobilities are obtained, separated by a critical current j_c (the so-called Walker current). Below j_c, the DW moves only along the nanostrip and does not rotate. The velocity increases linearly with the current with its mobility inversely proportional to the damping constant. This point is similar to the ferromagnetic case. Above j_c, the DW angle, the width, spiral pitch, and their rates of change, as well as the velocity, all vary periodically. In the high-current regime, the average velocity and angular velocity scale linearly with the current.

Combining the adjustability of FiM with the spatial twist produced by DMI, more abundant dynamics arise for the spiral FiM DWs, such as reversal of the DW propagation and rotation, change of the magnitude of (angular) velocity, and switching of spiral chirality. We envision that these features can enrich the study of the DW dynamics and provide a clue for future experiments of FiM.

APPENDIX A: DERIVATIONS FROM m₁-m₂ EQUATIONS TO REDUCED l-EQUATION

We consider a ferrimagnetic metallic nanowire with a bulk DMI and a longitudinal easy axis defined as z axis, as shown in Fig. 1. A longitudinal electric current flows through the strip, generating adiabatic and nonadiabatic STTs. Phenomenologically, the current-driven ferrimagnetic dynamics can be described by two exchange-coupled LLG equations written as

$$\frac{\partial \mathbf{m}_i}{\partial t} = \frac{\gamma_i}{M_i}\mathbf{m}_i \times \frac{\delta E}{\delta \mathbf{m}_i} + \alpha_i \mathbf{m}_i \times \frac{d\mathbf{m}_i}{dt} + \frac{\gamma_i}{M_i}\mathbf{T}_i, \quad (A1)$$

where $\mathbf{m}_i$ and M_i are the unit vectors and the magnitudes of sublattice magnetization, with $i = 1, 2$, representing the magnetic moment of transition metal and that of rare metal, respectively. γ_i are the gyromagnetic ratios and equal to $g_i\frac{\mu_B}{\hbar}$, with g_i being the Landé factors, μ_B the Bohr magneton, and $\hbar$ the reduced Planck constant. The magnetic energy includes the contributions from the exchange interaction, magnetic anisotropy, demagnetization, and DMI,

$$E = \int (\mathcal{E}_{ex} + \mathcal{E}_{an} + \mathcal{E}_{de} + \mathcal{E}_{dm})d\mathbf{r}. \quad (A2)$$

Here the exchange energy density is

$$\mathcal{E}_{ex} = 2A_0\mathbf{m}_1 \cdot \mathbf{m}_2 + A_1\mathbf{m}_2 \cdot \frac{\partial \mathbf{m}_1}{\partial z} + A_2\mathbf{m}_2 \cdot \frac{\partial^2 \mathbf{m}_1}{\partial z^2}, \quad (A3)$$

where $A_0 = \mathsf{J}/\Omega$, $A_1 = (\mathsf{J}/\Omega)a$, and $A_2 = (\mathsf{J}/\Omega)a^2/2$, with $\mathsf{J} > 0$ being the exchange energy between a pair of nearest magnetic moments, Ω the volume of unit cell, and a the lattice constant along the z axis. The anisotropy energy density is

$$\mathcal{E}_{an} = -K_1(\mathbf{m}_1 \cdot \mathbf{e}_z)^2 - K_2(\mathbf{m}_2 \cdot \mathbf{e}_z)^2, \quad (A4)$$

with K_i being anisotropy constants. The demagnetization energy density is

$$\mathcal{E}_{de} = \tfrac{1}{2}N_x\mu_0[(M_1\mathbf{m}_1 + M_2\mathbf{m}_2) \cdot \mathbf{e}_x]^2 + \tfrac{1}{2}N_y\mu_0[(M_1\mathbf{m}_1 + M_2\mathbf{m}_2) \cdot \mathbf{e}_y]^2, \quad (A5)$$

with μ_0 being the vacuum magnetic conductivity, and $N_{x,y}$ the demagnetization factors. For long magnetic nanostrips, the demagnetization along the z axis is almost zero. So we consider only the demagnetization along x and y axes, and $N_x + N_y = 1$. The DMI energy density is

$$\mathcal{E}_{dm} = D\mathbf{e}_z \cdot \left(\mathbf{m}_2 \times \frac{\partial \mathbf{m}_1}{\partial z}\right), \quad (A6)$$

where $D = (\mathsf{D}/\Omega)a$, with D being the DMI energy between a pair of nearest magnetic moments. The spin-transfer torques, including the adiabatic and nonasiabatic terms, read

$$\mathbf{T}_i = -P_i j_e \mathbf{m}_i \times \left(\mathbf{m}_i \times \frac{\partial \mathbf{m}_i}{\partial z}\right) - \beta P_i j_e \mathbf{m}_i \times \frac{\partial \mathbf{m}_i}{\partial z}, \quad (A7)$$

where j_e is the current density, β is the nonadiabatic constant, and $P_i = \frac{\hbar}{2e}p_i$, with p_i being the spin polarizations and e the elementary charge.

Introducing the density of angular moment $S_i = M_i/\gamma_i$, the coupled LLG equations are explicitly expressed as

$$S_i\frac{\partial \mathbf{m}_i}{\partial t} = \mathbf{m}_i \times \left(2A_0\mathbf{m}_{3-i} + (-1)^i A_1\frac{\partial \mathbf{m}_{3-i}}{\partial z} + A_2\frac{\partial^2 \mathbf{m}_{3-i}}{\partial z^2}\right) - D\mathbf{m}_i \times \left(\mathbf{e}_z \times \frac{\partial \mathbf{m}_{3-i}}{\partial z}\right) - K_i(\mathbf{m}_i \cdot \mathbf{e}_z)(\mathbf{m}_i \times \mathbf{e}_z)$$
$$+ N_x\mu_0 M_i[(M_1\mathbf{m}_1 + M_2\mathbf{m}_2) \cdot \mathbf{e}_x](\mathbf{m}_i \times \mathbf{e}_x) + + N_y\mu_0 M_i[(M_1\mathbf{m}_1 + M_2\mathbf{m}_2) \cdot \mathbf{e}_y](\mathbf{m}_i \times \mathbf{e}_y)$$
$$+ \alpha_i S_i\mathbf{m}_i \times \frac{\partial \mathbf{m}_i}{\partial t} - P_i j_e\left[\mathbf{m}_i \times \left(\mathbf{m}_i \times \frac{\partial \mathbf{m}_i}{\partial z}\right) + \beta\mathbf{m}_i \times \frac{\partial \mathbf{m}_i}{\partial z}\right]. \quad (A8)$$

To deal with the ferrimagnetic dynamics analytically, it is convenient to introduce a reduced magnetization $\mathbf{m} = 1/2(\mathbf{m}_1 + \mathbf{m}_2)$, and a Néel order parameter $\mathbf{l} = 1/2(\mathbf{m}_1 - \mathbf{m}_2)$. Obviously, $\mathbf{l} \cdot \mathbf{m} = 0$ and $\mathbf{l}^2 + \mathbf{m}^2 = 1$. In the ground state, $\mathbf{m} = 0$ and $|\mathbf{l}| = 1$. It is reasonable to assume that the exchange coupling between the transition metal and rare metal sublattices is strong enough to ensure a nearly antiparallel alignment. So, in the strong-exchange limit and near the ground state ($\mathbf{m}^2 \ll 1$), the coupled $\mathbf{m}_1$-$\mathbf{m}_2$ equations [Eq. (A8)] can be reduced as an $\mathbf{l}$-equation with $\mathbf{m}$ being a slave vector, i.e., Eqs. (1)–(4).

APPENDIX B: DYNAMIC EQUATIONS NEAR THE MAGNETIZATION COMPENSATION POINT

Due to the assumption $|\mathbf{l}| \approx 1$, it is convenient to parametrize $\mathbf{l}$ with spherical coordinates, namely, $\mathbf{l} = \sin\theta\cos\varphi\mathbf{e}_x + \sin\theta\sin\varphi\mathbf{e}_y + \cos\theta\mathbf{e}_z$ with θ and φ being the polar and azimuthal angles, respectively. Then Eq. (1) is transformed into

$$-\rho(\varphi_{tt}\sin\theta + 2\theta_t\varphi_t\cos\theta) - S_-\theta_t - \alpha S_+\varphi_t\sin\theta$$
$$= \frac{1}{\sin\theta}\frac{\delta E_l}{\delta\varphi} - P_- j_e\theta_z - \beta P_+ j_e\varphi_z\sin\theta, \quad (B1)$$

$$\rho(\theta_{tt} - \varphi_{tt}\sin\theta\cos\theta) - S_-\varphi_t\sin\theta + \alpha S_+\theta_t$$
$$= -\frac{\delta E_l}{\delta\theta} - P_- j_e\varphi_z\sin\theta + \beta P_+ j_e\theta_z, \quad (B2)$$

where the subscripts t and z indicate the derivative with respect to them. Correspondingly, the energy density is also expressed in spherical coordinates as

$$\mathcal{E}_l = \frac{A_2}{2}\left(\theta_z^2 + \sin^2\theta\varphi_z^2\right) - K\cos^2\theta - D\varphi_z\sin^2\theta$$
$$+ \frac{1}{2}\mu_0 M_-^2\sin^2\theta\left(N_x\cos\varphi^2 + N_y\sin^2\varphi\right). \quad (B3)$$
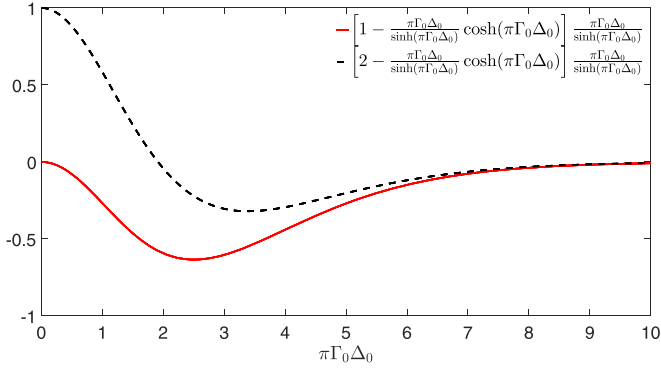
FIG. 6. Two functions about $\pi\Gamma_0\Delta_0$ in the terms of $\mu_0 M_-^2$ of Eqs. (B22) and (B23).

Near MCP, by reference to the static spiral Walker profile, the dynamic ansatz is written as

$$\theta = 2\arctan\exp\left[\lambda\frac{z-q(t)}{\Delta(t)}\right] \tag{B4}$$

$$\varphi = \Gamma(t)[z-q(t)] + \phi(t). \tag{B5}$$

Their temporal and spatial derivatives will be used in the following calculations and are derived as

$$\theta_t = -\lambda\frac{\dot{q}}{\Delta}\sin\theta - \frac{\dot{\Delta}}{\Delta}\sin\theta\ln\tan\frac{\theta}{2}, \tag{B6}$$

$$\theta_{tt} = -\lambda\frac{\ddot{q}}{\Delta}\sin\theta - \frac{\ddot{\Delta}}{\Delta}\sin\theta\ln\tan\frac{\theta}{2} + \frac{\dot{q}^2}{\Delta^2}\sin\theta\cos\theta$$
$$+ \frac{\dot{\Delta}^2}{\Delta^2}\sin\theta\ln\tan\frac{\theta}{2}\left(2+\cos\theta\ln\tan\frac{\theta}{2}\right)$$
$$+ \lambda\frac{\dot{q}}{\Delta}\frac{\dot{\Delta}}{\Delta}\sin\theta\left(1+\cos\theta\ln\tan\frac{\theta}{2}\right), \tag{B7}$$

$$\theta_z = \lambda\frac{1}{\Delta}\sin\theta, \tag{B8}$$

where the overdot denotes the derivative with respect to the time, and

$$\varphi_t = -\Gamma\dot{q} + \dot{\phi} + \lambda\Delta\dot{\Gamma}\ln\tan\frac{\theta}{2}, \tag{B9}$$

$$\varphi_{tt} = -\Gamma\ddot{q} + \ddot{\phi} + \lambda\Delta\ddot{\Gamma}\ln\tan\frac{\theta}{2} - 2\dot{q}\dot{\Gamma}, \tag{B10}$$

$$\varphi_z = \Gamma. \tag{B11}$$

In addition, the variations of θ and φ are expressed as

$$\delta\theta = -\lambda\frac{\delta q}{\Delta}\sin\theta - \frac{\delta\Delta}{\Delta}\sin\theta\ln\tan\frac{\theta}{2}, \tag{B12}$$

$$\delta\varphi = -\Gamma\delta q + \delta\phi + \lambda\Delta\delta\Gamma\ln\tan\frac{\theta}{2}. \tag{B13}$$

For convenience, Eqs. (B1) and (B2) can be written in a variational form,

$$\delta E_l = \frac{\delta E_l}{\delta\theta}\delta\theta + \frac{\delta E_l}{\delta\varphi}\delta\varphi, \tag{B14}$$

where

$$\frac{\delta E_l}{\delta\theta} = -\rho(\theta_{tt} - \varphi_{tt}\sin\theta\cos\theta) + S_-\varphi_t\sin\theta$$
$$- \alpha S_+\theta_t - P_- j_e\varphi_z\sin\theta + \beta P_+ j_e\theta_z, \tag{B15}$$

$$\frac{\delta E_l}{\delta\varphi} = -\rho\left(\varphi_{tt}\sin^2\theta + 2\theta_t\varphi_t\sin\theta\cos\theta\right) - S_-\theta_t\sin\theta$$
$$- \alpha S_+\varphi_t\sin^2\theta + P_- j_e\theta_z\sin\theta + \beta P_+ j_e\varphi_z\sin^2\theta. \tag{B16}$$

By using the dynamic ansatz Eqs. (B4) and (B5), the temporal and spatial derivatives of θ and φ, and the variations of θ and φ, integrating δE_l over z, the variation of DW energy per unit area, $\delta\sigma = \int_{-\infty}^{\infty}\delta E_l\,dz$, can be obtained by a direct and tedious calculation,

$$\delta\sigma = \frac{\delta\sigma}{\delta q}\delta q + \frac{\delta\sigma}{\delta\phi}\delta\phi + \frac{\delta\sigma}{\delta\Delta}\delta\Delta + \frac{\delta\sigma}{\delta\Gamma}\delta\Gamma, \tag{B17}$$

where $\delta\sigma/\delta q$, $\delta\sigma/\delta\phi$, $\delta\sigma/\delta\Delta$, and $\delta\sigma/\delta\Gamma$ are Eqs. (24)–(27).

On the other hand, inserting the ansatz (B4) and (B5) and the spatial derivatives θ_z and φ_z into Eq. (B3), and integrating over z, the energy per unit area of the plane of DW, Eq. (28), can be calculated by $\sigma = \int_{-\infty}^{\infty}\mathcal{E}_l dz$. Then, from Eq. (B17), we get the dynamic equations about the four collective coordinates,

$$\rho(1+\Gamma^2\Delta^2)\Delta^{-1}\ddot{q} - \rho\Gamma\Delta\ddot{\phi} - 1/2\rho\Delta\ddot{\Gamma} = -\alpha S_+(1+\Gamma^2\Delta^2)\Delta^{-1}\dot{q} - (\lambda S_- - \alpha S_+\Gamma\Delta)\dot{\phi} - \rho\Gamma\Delta\dot{q}\dot{\Gamma} - \rho(\Gamma^2 - \Delta^{-2})\dot{q}\dot{\Delta}$$
$$+ \rho\Gamma\dot{\phi}\dot{\Delta} - (1+\Gamma^2\Delta^2)\Delta^{-1}\beta P_+ j_e, \tag{B18}$$

$$\rho\Gamma\ddot{q} - \rho\ddot{\phi} = -(\lambda\Delta^{-1}S_- + \alpha\Gamma S_+)\dot{q} + \alpha S_+\dot{\phi} - \rho\dot{q}\dot{\Gamma} - \rho\Gamma\Delta^{-1}\dot{q}\dot{\Delta} + \rho\Delta^{-1}\dot{\Delta}\dot{\phi}$$
$$- 1/2(N_x - N_y)\mu_0 M_-^2\pi\Gamma\Delta\,\mathrm{csch}(\pi\Gamma\Delta)\sin 2\phi - (\lambda\Delta^{-1}P_- + \Gamma\beta P_+)j_e, \tag{B19}$$

$$\rho\Gamma\ddot{q} - \rho\ddot{\phi} + \pi^2/6\rho\Delta^{-1}\ddot{\Delta} = -\rho\Delta^{-2}\dot{q}^2 + \pi^2/12\rho\Delta^{-2}\dot{\Delta}^2 - \pi^2/6\alpha S_+\Delta^{-1}\dot{\Delta} - \pi^2/6\lambda S_-\Delta\dot{\Gamma} - 2\rho\dot{q}\dot{\Gamma} + A_2\Delta^{-2} - 2K - A_2\Gamma^2$$
$$+ 2D\Gamma - 1/2\mu_0 M_-^2\{1 + (N_x - N_y)[2 - \pi\Gamma\Delta\coth(\pi\Gamma\Delta)]\pi\Gamma\Delta\,\mathrm{csch}(\pi\Gamma\Delta)\cos 2\phi\}, \tag{B20}$$

$$\pi^2/6\rho\Delta^2\Gamma\ddot{\Gamma} = 2\rho\Gamma^2\dot{q}^2 + \pi^2/6\lambda S_-\Gamma\dot{\Delta} - \pi^2/6\alpha S_+\Delta^2\Gamma\dot{\Gamma} - \pi^2/2\rho\Gamma\Delta\dot{\Gamma}\dot{\Delta} - 2\rho\Gamma\dot{q}\dot{\phi}$$
$$- 2A_2\Gamma^2 + 2D\Gamma - 1/2(N_x - N_y)\mu_0 M_-^2[1 - \pi\Gamma\Delta\coth(\pi\Gamma\Delta)]\pi\Gamma\Delta\,\mathrm{csch}(\pi\Gamma\Delta)\cos 2\phi. \tag{B21}$$

Taking $\ddot{q}$, $\ddot{\phi}$, $\ddot{\Delta}$, $\ddot{\Gamma}$, $\dot{\phi}$, $\dot{\Delta}$, and $\dot{\Gamma}$ to be zero, Eqs. (29)–(31) can be inferred from Eqs. (B18) and (B19). From Eqs. (B20) and (B21), Δ_0 and Γ_0 satisfy

$$\Delta_0^2 = \frac{A_2 - \rho v_0^2}{2K + A_2\Gamma_0^2 - 2D\Gamma_0 + \frac{1}{2}\mu_0 M_-^2 \left\{1 + (N_x - N_y)\left[2 - \frac{\pi\Gamma_0\Delta_0}{\sinh(\pi\Gamma_0\Delta_0)}\cosh(\pi\Gamma_0\Delta_0)\right]\frac{\pi\Gamma_0\Delta_0}{\sinh(\pi\Gamma_0\Delta_0)}\cos 2\phi_0\right\}}, \quad \text{(B22)}$$

$$\Gamma_0^{-2} = \frac{A_2 - \rho v_0^2}{D\Gamma_0 - \frac{1}{4}(N_x - N_y)\mu_0 M_-^2 \left[1 - \frac{\pi\Gamma_0\Delta_0}{\sinh(\pi\Gamma_0\Delta_0)}\cosh(\pi\Gamma_0\Delta_0)\right]\frac{\pi\Gamma_0\Delta_0}{\sinh(\pi\Gamma_0\Delta_0)}\cos 2\phi_0}. \quad \text{(B23)}$$

Equations (B22) and (B23) are two coupled transcendental equations. It is impossible to obtain explicit expressions of Γ_0 and Δ_0 as a function of j_e. However, near the MCP, $\mu_0 M_-^2$ are much smaller than other terms in the denominator of these two equations. For example, $D\Gamma_0 \approx D\Gamma_s = D^2/A_2 = 6.01 \times 10^5$ J/m^3 and $\mu_0 M_-^2 = 1.04 \times 10^4$ J/m^3 for the used parameters. Furthermore, N_x, N_y, and $\cos 2\phi_0$ have the order of 1. As shown in Fig. 6, the two functions about $\pi\Gamma_0\Delta_0$ in the denominator of Eqs. (B22) and (B23) are smaller than 1. So it is reasonable to omit the terms of $\mu_0 M_-^2$ in Eqs. (B22) and (B23). Then Eqs. (32) and (33) are obtained.

[1] D. Allwood, G. Xiong, C. Faulkner, D. Atkinson, D. Petit, and R. Cowburn, Magnetic domain-wall logic, Science **309**, 1688 (2005).

[2] S. S. P. Parkin, M. Hayashi, and L. Thomas, Magnetic domain-wall racetrack memory, Science **320**, 190 (2008).

[3] A. C. Swaving, R. A. Duine, Current-induced torques in continuous antiferromagnetic textures, Phys. Rev. B **83**, 054428 (2011).

[4] K. M. D. Hals, Y. Tserkovnyak, and A. Brataas, Phenomenology of Current-Induced Dynamics in Antiferromagnets, Phys. Rev. Lett. **106**, 107206 (2011).

[5] E. G. Tveten, A. Qaiumzadeh, O. A. Tretiakov, and A. Brataas, Staggered Dynamics in Antiferromagnets by Collective Coordinates, Phys. Rev. Lett. **110**, 127208 (2013).

[6] D. R. Rodrigues, K. Everschor-Sitte, O. A. Tretiakov, J. Sinova, and A. Abanov, Spin texture motion in antiferromagnetic and ferromagnetic nanowires, Phys. Rev. B **95**, 174408 (2017).

[7] H. J. Park, Y. Jeong, S. H. Oh, G. Go, J. H. Oh, K. W. Kim, H. W. Lee, and K. J. Lee, Numerical computation of spin-transfer torques for antiferromagnetic domain walls, Phys. Rev. B **101**, 144431 (2020).

[8] J. J. Nakane and H. Kohno, Microscopic calculation of spin torques in textured antiferromagnets, Phys. Rev. B **103**, L180405 (2021).

[9] E. Haltz, S. Krishnia, L. Berges, A. Mougin, and J. Sampaio, Domain wall dynamics in antiferromagnetically coupled double-lattice systems, Phys. Rev. B **103**, 014444 (2021).

[10] O. Gomonay, T. Jungwirth, and J. Sinova, High Antiferromagnetic Domain Wall Velocity Induced by Néel Spin-Orbit Torques, Phys. Rev. Lett. **117**, 017202 (2016).

[11] T. Shiino, S. H. Oh, P. M. Haney, S. W. Lee, G. Go, B. G. Park, and K. J. Lee, Antiferromagnetic Domain Wall Motion Driven by Spin-Orbit Torques, Phys. Rev. Lett. **117**, 087203 (2016).

[12] Y. C. Liang, P. B. He, M. Q. Cai, and Z. D. Li, Motion and stability of chiral domain walls driven by non-gradient spin torques: Antiferromagnets and ferromagnets compared, J. Magn. Magn. Mater. **479**, 291 (2019).

[13] L. Sánchez-Tejerina, V. Puliafito, P. K. Amiri, M. Carpentieri, and G. Finocchio, Dynamics of domain-wall motion driven by spin-orbit torque in antiferromagnets, Phys. Rev. B **101**, 014433 (2020).

[14] P. Hansen, C. Clausen, G. Much, M. Rosenkranz, and K. Witter, Magnetic and magneto-optical properties of rare-earth transition-metal alloys containing Gd, Tb, Fe, Co, J. Appl. Phys. **66**, 756 (1989).

[15] K. J. Kim, S. K. Kim, Y. Hirata, S. H. Oh, T. Tono, D. H. Kim, T. Okuno, W. S. Ham, S. Kim, G. Go, Y. Tserkovnyak, A. Tsukamoto, T. Moriyama, K. J. Lee, and T. Ono, Fast domain wall motion in the vicinity of the angular momentum compensation temperature of ferrimagnets, Nat. Mater. **16**, 1187 (2017).

[16] S. A. Siddiqui, Jiahao Han, J. T. Finley, C. A. Ross, and L. Liu, Current-Induced Domain Wall Motion in a Compensated Ferrimagnet, Phys. Rev. Lett. **121**, 057701 (2018).

[17] L. Caretta, M. Mann, F. Büttner, K. Ueda, B. Pfau, C. M. Günther, P. Hessing, A. Churikova, C. Klose, M. Schneider, D. Engel, C. Marcus, D. Bono, K. Bagschik, S. Eisebitt, and G. S. D. Beach, Fast current-driven domain walls and small skyrmions in a compensated ferrimagnet, Nat. Nanotechnol. **13**, 1154 (2018).

[18] C. O. Avci, E. Rosenberg, L. Caretta, F. Büttner, M. Mann, C. Marcus, D. Bono, C. A. Ross, and G. S. D. Beach, Interface-driven chiral magnetism and current-driven domain walls in insulating magnetic garnets, Nat. Nanotechnol. **14**, 561 (2019).

[19] S. Ghosh, T. Komori, A. Hallal, J. P. Garcia, T. Gushi, T. Hirose, H. Mitarai, H. Okuno, J. Vogel, M. Chshiev, J. P. Attané, L. Vila, T. Suemasu, and S. Pizzini, Current-Driven Domain Wall Dynamics in Ferrimagnetic Nickel-Doped Mn$_4$N Films: Very Large Domain Wall Velocities and Reversal of Motion Direction across the Magnetic Compensation Point, Nano Lett. **21**, 2580 (2021).

[20] T. Okuno, D. H. Kim, S. H. Oh, S. K. Kim, Y. Hirata, T. Nishimura, W. S. Ham, Y. Futakawa, H. Yoshikawa, A. Tsukamoto, Y. Tserkovnyak, Y. Shiota, T. Moriyama, K. J. Kim, K. J. Lee, and T. Ono, Spin-transfer torques for domain wall motion in antiferromagnetically coupled ferrimagnets, Nat. Electron **2**, 389 (2019).

[21] E. Haltz, J. Sampaio, R. Weil, Y. Dumont, and A. Mougin, Strong current actions on ferrimagnetic domain walls in the creep regime, Phys. Rev. B **99**, 104413 (2019).

[22] S. H. Oh, S. K. Kim, J. Xiao, and K. J. Lee, Bidirectional spin-wave-driven domain wall motion in ferrimagnets, Phys. Rev. B **100**, 174403 (2019).

[23] W. H. Li, Z. Jin, D. L. Wen, X. M. Zhang, M. H. Qin, and J.-M. Liu, Ultrafast domain wall motion in ferrimagnets induced by magnetic anisotropy gradient, Phys. Rev. B **101**, 024414 (2020).

[24] S.-H. Oh and K.-J. Lee, Ferrimagnetic domain wall motion induced by damping-like spin-orbit torque, J. Magn. **23**, 196 (2018).

[25] E. Martínez, V. Raposo, and Ó. Alejos, Current-driven domain wall dynamics in ferrimagnets: Micromagnetic approach and collective coordinates model, J. Magn. Magn. Mater. **491**, 165545 (2019).

[26] L. Sánchez-Tejerina, R. Tomasello, V. Puliafito, B. Azzerboni, M. Carpentieri, and G. Finocchio, Unified framework for micromagnetic modeling of ferro-, ferri-, and antiferromagnetic materials at mesoscopic scale: Domain wall dynamics as a case study, IEEE Magn. Lett. **11**, 2505005 (2020).

[27] V. V. Yurlov, K. A. Zvezdin, P. N. Skirdkov, and A. K. Zvezdin, Domain wall dynamics of ferrimagnets influenced by spin current near the angular momentum compensation temperature, Phys. Rev. B **103**, 134442 (2021).

[28] D. H. Kim, D. H. Kim, K. J. Kim, K. W. Moon, S. Yang, K. J. Lee, and S. K. Kim, The dynamics of a domain wall in ferrimagnets driven by spin-transfer torque, J. Magn. Magn. Mater. **514**, 167237 (2020).

[29] R. Lavrijsen, A new twist for spin torques in antiferromagnets, Nat. Electron **2**, 372 (2019).

[30] O. A. Tretiakov and A. Abanov, Current Driven Magnetization Dynamics in Ferromagnetic Nanowires with a Dzyaloshinskii-Moriya Interaction, Phys. Rev. Lett. **105**, 157201 (2010).

[31] F. Zhou and Z. Z. Sun, Field-driven domain wall motion in ferromagnetic nanowires with bulk Dzyaloshinskii-Moriya interaction, Sci. Rep. **6**, 25122 (2016).

[32] A. Thiaville, S. Rohart, É. Jué, V. Cros, and A. Fert, Dynamics of Dzyaloshinskii domain walls in ultrathin magnetic films, Europhys. Lett. **100**, 57002 (2012).

[33] H. Yan, P. B. He, M. Q. Cai, and Z. D. Li, Dynamics of chiral domain wall under the spin-orbit torques in heavy metal/ferromagnet bilayers with in-plane anisotropy, J. Magn. Magn. Mater. **441**, 691 (2017).

[34] M. Li, B. Xi, Y. J. Liu, and J. Lu, Enhancement of the Walker limit by bulk Dzyaloshinskii-Moriya interaction, Phys. Rev. B **105**, 014440 (2022).

[35] S. Krishnia, E. Haltz, L. Berges, L. Aballe, M. Foerster, L. Bocher, R. Weil, A. Thiaville, J. Sampaio, and A. Mougin, Spin-orbit coupling in single-layer ferrimagnets: Direct observation of spin-orbit torques and chiral spin textures, Phys. Rev. Appl. **16**, 024040 (2021).

[36] D. H. Kim, M. Haruta, H. W. Ko, G. Go, H. J. Park, T. Nishimura, D. Y. Kim, T. Okuno, Y. Hirata, Y. Futakawa, H. Yoshikawa, W. Ham, S. Kim, H. Kurata, A. Tsukamoto, Y. Shiota, T. Moriyama, S. B. Choe, K. J. Lee, and T. Ono, Bulk Dzyaloshinskii–Moriya interaction in amorphous ferrimagnetic alloys, Nat. Mater. **18**, 685 (2019).

[37] A. P. Malozemoff and J. C. Slonczewski, *Magnetic Domain Walls in Bubble Materials* (Academic Press, San Diego, 1979), pp. 123–127.

[38] A. Thiaville and Y. Nakatani, Domain-wall dynamics in nanowires and nanostrips, *Spin Dynamics in Confined Magnetic Structures III*, edited by B. Hillebrands and A. Thiaville (Springer, New York, 2002), pp. 177–187.

[39] J. X. Du, M. Li, and J. Lu, Stabilizing current-driven steady flows of 180° domain walls in spin valves by interfacial Dzyaloshinskii-Moriya interaction, Phys. Rev. B **103**, 144429 (2021).

[40] V. P. Kravchuk, Influence of Dzialoshinskii-Moriya interaction on static and dynamic properties of a transverse domain wall, J. Magn. Magn. Mater. **367**, 9 (2014).

[41] G. Tatara and H. Kohno, Theory of Current-Driven Domain Wall Motion: Spin Transfer versus Momentum Transfer, Phys. Rev. Lett. **92**, 086601 (2004).

[42] S. Zhang and Z. Li, Roles of Nonequilibrium Conduction Electrons on the Magnetization Dynamics of Ferromagnets, Phys. Rev. Lett. **93**, 127204 (2004).

[43] A. Thiaville, Y. Nakatani, J. Miltat, and Y. Suzuki, Micromagnetic understanding of current-driven domain wall motion in patterned nanowires, Europhys. Lett. **69**, 990 (2005).

[44] S. K. Kim, K. J. Lee, and Y. Tserkovnyak, Self-focusing skyrmion racetracks in ferrimagnets, Phys. Rev. B **95**, 140404(R) (2017).

[45] D. H. Kim, S. H. Oh, D. K. Lee, S. K. Kim, and K. J. Lee, Current-induced spin-wave Doppler shift and attenuation in compensated ferrimagnet, Phys. Rev. B **103**, 014433 (2021).